1) *dmin* = *d*, for case fig. 5(a);
2) *dmin* = $b_i m_{i+1}$, for case fig. 5(b);
3) *dmin* = $b_i m_{i+1}$, for case fig. 5(c);
4) *dmin* = $b_i b_{i+1}$, for case fig. 5(d).

The common normal line ($c_i c_{i+1}$) of line segment $a_i b_i$ and $a_{i+1} b_{i+1}$ could be expressed by eq.(11).

$$d = \left| (\mathbf{b}_i - \mathbf{b}_{i+1}) \mathrm{g} \frac{(\mathbf{b}_i - \mathbf{a}_i) \times (\mathbf{b}_{i+1} - \mathbf{a}_{i+1})}{\left\| (\mathbf{b}_i - \mathbf{a}_i) \times (\mathbf{b}_{i+1} - \mathbf{a}_{i+1}) \right\|} \right| \qquad (i = 1 \sim 6) \tag{11}$$

Where $\boldsymbol{a}_i$, $\boldsymbol{b}_i$, $\boldsymbol{a}_{i+1}$ and $\boldsymbol{b}_{i+1}$ were the vectors described in the fix *Cartesian* frame.

Let **m** be the vector along $\boldsymbol{a}_i \boldsymbol{b}_i$. It could be expressed by the parametric equation, see eq.(12). Meanwhile, the feet of perpendicular c_i and c_{i+1} could be obtained by solving eq.(13).

$$\mathbf{m}_i = \mathbf{a}_i + k_i (\mathbf{b}_i - \mathbf{a}_i) \qquad (i = 1 \sim 6) \tag{12}$$

$$\begin{cases} [\mathbf{a}_i + k_i (\mathbf{b}_i - \mathbf{a}_i) - \mathbf{a}_{i+1} - k_{i+1} (\mathbf{b}_{i+1} - \mathbf{a}_{i+1})] \mathrm{g} (\mathbf{a}_i - \mathbf{b}_i) = 0 \\ [\mathbf{a}_i + k_i (\mathbf{b}_i - \mathbf{a}_i) - \mathbf{a}_{i+1} - k_{i+1} (\mathbf{b}_{i+1} - \mathbf{a}_{i+1})] \mathrm{g} (\mathbf{a}_{i+1} - \mathbf{b}_{i+1}) = 0 \end{cases} \qquad (i = 1 \sim 6) \tag{13}$$

Unless $k_i \in [0, 1]$, point m_i lied between the points a_i and b_i; unless $k_{i+1} \in [0,1]$, point m_{i+1} lied between the points a_{i+1} and b_{i+1}. Let $b_i M_{i+1}$ be the perpendicular line of $a_{i+1} b_{i+1}$. m_{i+1} could be derived from eq. (14). Detailed flow chart of the contact interference was shown in fig. 6.

$$[\mathbf{b}_i - \mathbf{a}_{i+1} - m_{i+1} (\mathbf{b}_{i+1} - \mathbf{a}_{i+1})] \mathrm{g} (\mathbf{b}_{i+1} - \mathbf{a}_{i+1}) = 0 \qquad (i = 1 \sim 6) \tag{14}$$

3.1.2 Structure parameters and workplace of MLD

Based on the inverse kinematics and the interference boundary condition, structure parameters and the position workspace were obtained. Optimized parameters were summarized in table 1; different views of the position workspace were plotted in fig. 7, respectively. Different from the serial mechanism, the position and orientation workspaces of the parallel mechanism possessed strong coupled effects with each other. Consequently, the pose workspace usually be expressed by specific engineering performance indexes. As for this *MLD*, the pose workspace could be described that the orientation space should be as large as possible under the premise of meeting the requirements of the position space, see table 2.

Table 1. Structure parameters of the *MLD*.

Structure parameters	Value
r [mm]	120.00
R [mm]	175.86
β [°]	22.50
δ [°]	34.46
Initial length of L[mm]	370.00

Table 2. Pose workspace of the *MLD*.

Pose workspace parameters	Value
X [mm]	±40
Y [mm]	±40
Z [mm]	410～440
X [°]	-8～8
Y [°]	-8～8
Z [°]	-8～8

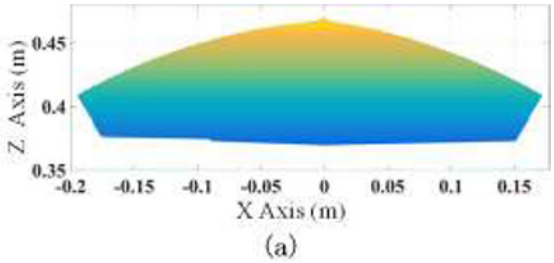

Figure 7. Different views of the position space.

3. Material mechanical experiments

Since the mobile platform of this *MLD* had six degrees of freedom, it could act more general loads on the material specimen, such as F_x, F_y, F_z, M_x, M_y, and M_z. As for this mechanism, as long as the *MLD* possessed enough stiffness, strength, motion space, and measurement accuracy, it could be used as a material testing machine. Translations and rotations along the three axes of the fixed *Cartesian* frame were the same in mechanism theory. Therefore, only tensile tests were performed to verify the loading capacity in this paper. In this work, specimen was manufactured using *AISI* 1045 steel widely used in practical application. All samples were referenced

Figure 8. Specimen geometry.

to the *Chinese* national standard *GB/T* 10128-2007, see fig. 8. Chemical composition of the specimen was 97.2%Fe, 0.46% C, 0.24% Si, 0.45% Mn, 0.015% Cr, 0.08% P, 0.003% S, ⩾0.01% Co, and 0.01% Ni. The measured average hardness of these specimen was 209.17HB.

Five repeated tensile tests were conducted on the *MLD* and the standard tensile testing machine Zwick Z100 according to the *Chinese* national standard *GB/T* 10128-2007, respectively. Experimental photos of these two devices were shown in fig. 9, and fig. 10. Stress-train curves obtained from these tests were plotted in fig. 11 and fig. 12, respectively.

Figure 9. Tensile tests on the *MLD*.

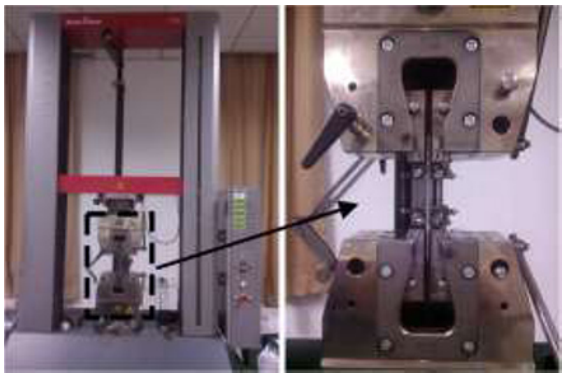

Figure 10. Tensile tests on the Zwick Z100.

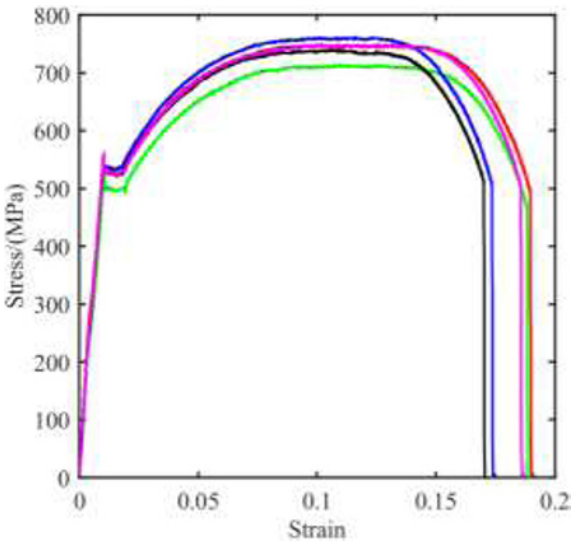

Figure 11. Stress-strain curves based on *MLD*.

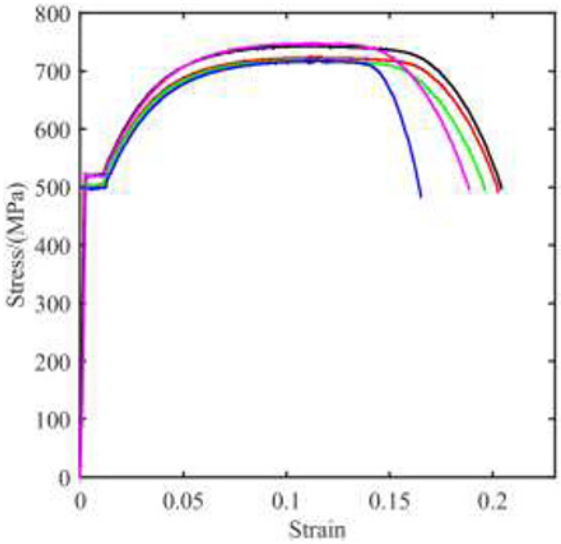

Figure 12. Stress-strain curves based on Zwick Z100.

Table 3. Comparison of mechanical properties derived from *MLD* and Zwick Z100.

Mechanical properties	*MLD* tests	Zwick Z100 tests	Error [%]
Average yield strength σ_s [Mpa]	521.36	515.52	1.13
Average ultimate strength σ_b [Mpa]	737.64	729.40	1.13

Mechanical properties derived from the two testers were compared and summarized in table 3.

Errors of the elastic segment in fig. 11 and fig. 12 were caused by that extensometer was not installed on the *MLD* while Zwick Z100 possessed an extensometer. Meanwhile, table 3 manifested that the maximum errors of σ_s and σ_b were merely both 1.13%. Therefore, results indicated that it was feasible to conduct material mechanical experiments on the *MLD*.

4. Summary

Aiming at the defects of the traditional material testers, on which the more general loads could not be applied, a new material mechanical *MLD* based on the parallel mechanism was proposed. Meanwhile, pure tensile experiments of *AISI* 1045 steel were performed on the *MLD* and on the standard tensile tester Zwick Z100, respectively. Main conclusions could be drawn as follows:

(1) Detailed contact interference boundary conditions were analysed which could be applied to the design of the parallel mechanism;

(2) The method of designing and optimizing structure parameters of the parallel mechanism was proposed based on the inverse kinematics and the contact interference boundary condition;

(3) Errors of the average yield and ultimate strengths obtained from the two devices were merely both 1.13%.

Results indicated that the *MLD* could meet the demands of material mechanical testing machine. It was feasible to perform material mechanical experiments via parallel mechanism.

5. Acknowledgements

All of the experiments described herein were supported by the AVIC industry-academy-research cooperation project (CXY2013BH05).

References

[1] F.Y. Zhou, Z.Y. Mao, *Engineering materials and application*, second ed., Huazhong University of science and technology, Wuhan, (2002).
[2] Z.H. Shan, *Mechanics of material*, third ed., Higher education press, Beijing, (2009).
[3] W.M. Lu, *Advanced strength and applied stress analysis*., Tsinghua university, Beijing, (2001).
[4] G.P.Z, *Experimental foundation of material mechanics*, first ed., Harbin institute technology, Harbin, (2010).
[5] J.J. H, M.G. Lee, F. Barlat, Strain hardening response and modelling of EDDQ and DP780 steel sheet under non-linear strain path, Mech Mater. **64**(2013) 11-26.
[6] S. Bruschi, T. Altan, Testing and modelling of material behaviour and formability in sheet metal forming, CIRP Annals. **63**(2014) 727-749.
[7] M.M. Rodr ́guez, R.A. Vaz, A. Arias, Failure behaviour of 2024-T3 aluminium under tension-torsion conditions, J. Mech Sci Technol. **29**(2015) 4657-4663.
[8] G.H. Zhao, L.B. Liu, Mechanical properties of AISI 1045 steel subjected to combined loads of tension and torsion, Exp Tech. **42** (2018) 393-406.
[9] J.Z. Guo, D. Wang, Development of a material testing machine with multi-dimensional loading capability, JSME. **10**(2016) JAMDSM0017-JAMDSM0017.